The Global Wind Atlas: A high-resolution dataset of climatologies and associated web-based application

Davis, Neil N.; Badger, Jake; Hahmann, Andrea N.; Hansen, Brian O.; Mortensen, Niels G.; Kelly, Mark; Larsén, Xiaoli G.; Olsen, Bjarke T.; Floors, Rogier; Lizcano, Gil

Total number of authors:
22

Published in:
Bulletin of the American Meteorological Society

Link to article, DOI:
10.1175/BAMS-D-21-0075.1

Publication date:
2023

Document Version
Peer reviewed version

The Global Wind Atlas: A high-resolution dataset of climatologies and associated web-based application

Neil N. Davis,[a] Jake Badger,[a] Andrea N. Hahmann,[a] Brian O. Hansen,[a] Niels G. Mortensen,[a] Mark Kelly,[a] Xiaoli G. Larsén,[a] Bjarke T. Olsen,[a] Rogier Floors,[a] Gil Lizcano,[b] Pau Casso,[b] Oriol Lacave,[b] Albert Bosch,[b] Ides Bauwens,[c] Oliver James Knight,[d] Albertine Potter van Loon,[d] Rachel Fox,[d] Tigran Parvanyan,[d] Søren Bo Krohn Hansen,[e] Duncan Heathfield,[f] Marko Onninen,[f] and Ray Drummond[f]

[a] *Technical University of Denmark, Department of Wind and Energy Systems, Roskilde, Denmark*

[b] *Vortex FDC, Barcelona, Spain*

[c] *Nazka Mapps, Leuven, Belgium*

[d] *World Bank Group, Washington D.C., USA*

[e] *Søren Krohn Consulting, Holte, Denmark*

[f] *World in a Box, Karkkila, Finland*

Corresponding author: Neil Davis, neda@dtu.dk

Early Online Release: This preliminary version has been accepted for publication in *Bulletin of the American Meteorological Society*, may be fully cited, and has been assigned DOI 10.1175/BAMS-D-21-0075.1. The final typeset copyedited article will replace the EOR at the above DOI when it is published.

ABSTRACT: The Global Wind Atlas (GWA) provides high-resolution databases and maps of the wind resource for all land points within 200 km of the coastline, excluding Antarctica. The GWA is used to identify and understand the global, national, regional, and local potential for wind energy and to guide energy specialists, policymakers, and planners in the transition to a sustainable energy system. This information is vital to ensuring the growth of wind energy, helping to transition to a sustainable energy system, which will mitigate climate change and meet the world's need for reliable, affordable, and clean energy. The GWA uses the established numerical wind atlas methodology to downscale coarse-resolution wind data to microscale, using linearized flow modeling and high-resolution topographic data. There have been three versions of the GWA, each using mesoscale model data at successively higher spatial resolution. A website and Geographic Information System (GIS) files support quick and in-depth analysis. Validation data and analysis, using measurements from tall masts located worldwide, are also provided through the web application. The development process of the GWA involves a dialogue between meteorological modelers, wind energy development experts, web designers, and representatives of the end-users to provide accurate data in a dynamic and relevant way. This article outlines the general method, specific development, and application of the Global Wind Atlas.

Accepted for publication in *Bulletin of the American Meteorological Society.* DOI 10.1175/BAMS-D-21-0075.1.

CAPSULE: The Global Wind Atlas provides an accurate high-resolution climatology of the wind resource based on state-of-the-art modeling, via a web-interface.

1. Introduction

To help mitigate climate change, thousands upon thousands of wind turbines need to be installed every year for decades (IEA 2021). Wind resource varies greatly from place to place, and even at the wind farm project pre-feasibility stage, reliable wind climates are required to define project specifications and determine their economic feasibility. To support this, high-resolution databases and maps of the wind resource (wind atlases) are needed, which allow users to identify areas of potential wind installations and calculate the expected electricity production. While coarse resolution global datasets, including reanalysis data, have also been used for global wind resource assessment, partly due to their availability and coverage, their coarse grid spacing of 50–100 km, means they cannot accurately represent the wind conditions at the detail typically required for wind energy deployment. In addition to high spatial variability, the wind resource has a height-dependent sensitivity to changes in elevation and aerodynamic surface roughness (e.g. Lee and Fields 2021). The resolution sensitivity is typically greater at windier sites, where wind turbines are often deployed. As an example of this effect, Fig. 1 shows the power density of a relatively hilly 200 km × 200 km area at two different model resolutions (dx = 3000 m and dx = 100 m). The figure shows that the windiest sites have significantly more wind resource in the higher resolution map than in the lower resolution map. This means that while developments in reanalysis data have helped the endeavor toward global wind mapping, their coarse grid spacing of 25–100 km means that they are still not suitable for accurate assessment of the wind resources.

Until recently, high-resolution wind atlases were only available on national and continental scales. This meant that many areas remained uncovered, and even if a country did have a wind resource map, it might be based on a different methodology, and have a different set of output specifications (e.g. output at different resolution, at different heights above surface, etc), which hindered intercomparison. This led to a desire from many potential users for a compatible set of data across different countries.

For these reasons, the Global Wind Atlas (GWA) was created, with a common methodology and data output specifications across the globe. This article outlines the developments of the GWA in

Accepted for publication in *Bulletin of the American Meteorological Society.* DOI 10.1175/BAMS-D-21-0075.1.

the ways that it was generated and used to present, and communicate the wind climatology and resources to different end users.

It is believed that most users fall into two main groups. The first is composed of energy generalists, who wish to quickly access summary data, graphics, and analysis, to incorporate wind energy related data into a broader energy context. The second group is composed of wind energy experts, who wish to access detailed datasets based on state-of-the-art methodologies, to either obtain a first screening assessment or compare to their own results as part of an ensemble or suite of methodologies.

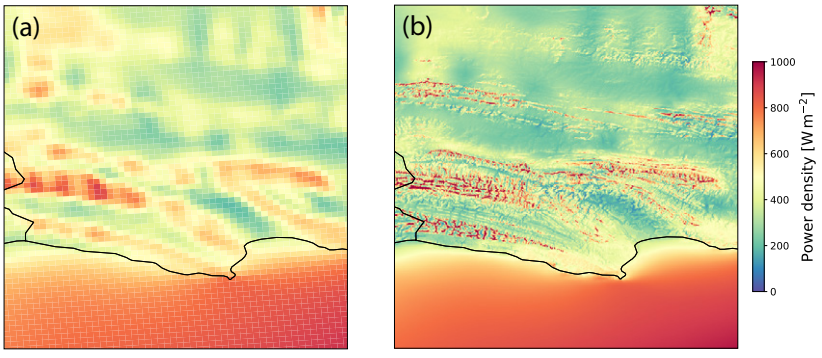

FIG. 1. Comparison of an assessment of wind power density for the same area using models at different resolutions, from Hahmann et al. (2021): mean wind power density calculated using results from a mesoscale simulation with grid spacing of 3,000 m (a), and the numerical wind atlas methodology to a grid spacing of 100 m (b). The higher resolution model is better able to capture features in the terrain that impact wind speeds. It can be shown that even if the mean wind speed for the area remains unchanged, the increased variance of mean wind speed is associated with an increase in wind power density for the same area. For the areas where the wind speeds are positively impacted by high resolution terrain features, the impact on wind power density can be dramatic.

The first GWA was released in 2015, providing kilometer-scale wind resource estimates (aggregated from results with grid spacing of 250 m) for all land and near coastal points, except for Antarctica. The development of the GWA was enabled by several factors, most notably the avail-

Accepted for publication in *Bulletin of the American Meteorological Society*. DOI 10.1175/BAMS-D-21-0075.1.

ability of relatively high-resolution global reanalysis datasets, high-resolution global space-based topographic data, increased computational power, and the development of the Numerical Wind Atlas (NWA) approach, described in section 2. In the nearly seven years since the release of the first GWA, two subsequent releases have been made, focused on improving the dynamic (mesoscale) wind data through the use of higher resolution Numerical Weather Prediction (NWP) modeling.

The NWA method provides a rich dataset, going well beyond maps alone. To help users explore this rich data, the GWA was developed with an interactive website right from the start. The dedicated websites provide an easy-to-use view of the data, and can work as an initial screening tool for the wind energy community. More complex analyses and improved download capabilities have been added over time, allowing the user to take their work from the website into their own tools and in some cases even load it back again. At the time of writing (Jan 2023), the GWA website has hosted over 1.9 million sessions from 236 countries, dependent territories, or special areas of geographical interest[1], and in the last year it has exceeded 30 thousand users per month.

This paper discusses the evolution of the GWA and its current capabilities, providing a view into the data, methods, and validation of each version. Section 2 provides an introduction to the Numerical Wind Atlas method, which is used to perform the microscale downscaling in the GWA. Section 3 provides an overview of the model configuration and input data to the model chains of the different versions of the GWA. An overview of the validation using tall-mast data from a few countries is provided in section 4, while examples of how the GWA can be used are presented in section 5. Finally, conclusions and further developments are given in section 6.

2. Numerical Wind Atlas Method

Central to the GWA is the Numerical Wind Atlas method. The method, introduced in Frank and Landberg (1997), builds on the observation-based wind atlas methodology, which was developed for the Danish Wind Atlas (Lundtang Petersen et al. 1981) and then the European Wind Atlas (Troen and Petersen 1989), and implemented in the WAsP software (Troen 1990; Landberg et al. 2003; Mortensen et al. 2006; Floors and Nielsen 2019) released along-side. Figure 2 shows the basic workflow of the NWA method, which consists of two main downscaling steps. The first uses a mesoscale model to capture additional flow phenomena, typically on the kilometer to tens of kilometer scales, not included in the input Reanalysis datasets. This is followed by a microscale

[1]Derived from analytics based on ISO 2-character codes https://en.wikipedia.org/wiki/ISO_3166-1_alpha-2

Accepted for publication in *Bulletin of the American Meteorological Society.* DOI 10.1175/BAMS-D-21-0075.1.

downscaling, which typically focuses on local topographic effects. The main topographic effects captured in the WAsP microscale model are the speedup of the wind due to orographic and surface roughness changes, the turning of the wind due to orography, and the change of the vertical profile due to changes in the background surface roughness.

The concept of a "wind climate" is central to the NWA method. A wind climate represents the wind as a multi-dimensional distribution, binned by both direction and speed. The directional bins are called sectors, and for the GWA always span 30°, leading to 12 sectors. The wind speed is initially grouped into 1 $\mathrm{m\,s^{-1}}$ bins, which are then fit to a Weibull distribution for use with the WAsP model. The Weibull parameters are consistent with employing the geostrophic drag law (GDL) using a single set of constants applicable over land and sea (see e.g. van der Laan et al. 2020), and enable vertical extrapolation based on either observations or models. Weibull distributions are found to reliably fit wind distributions for sufficiently narrow directional sectors (such as the 30° used herein), which is why they have been used for decades in wind energy applications.

As part of the microscale downscaling, a generalized wind climate (GWC) is used to relate the mesoscale and microscale wind climates, by defining a wind climate at a set of standard surface conditions, which are defined as a constant elevation and surface roughness. The GWA is calculated by using the geostrophic drag law (see Appendix A) to relate near-surface winds, associated with one set of surface conditions, to the expected near-surface winds associated with a standard set of surface conditions. This process can be thought of as a standardization framework for wind statistics, to remove the impacts of orography and roughness length changes, based on the GDL (see Appendix A for details).

Applying the generalization process to wind climates from coarser models, such as the reanalysis data for GWA1 and mesoscale data in GWA2 and GWA3, removes biases in the wind climate related to the under-resolved topographic effects related to the coarse model resolution (Badger et al. 2014; Hahmann et al. 2014). These biases include underestimation of the slope of hills and valleys, and abrupt misplacement, due to discretization, of the location of coastlines and other land cover features that impact the surface aerodynamic roughness length (z_0). Imperfections in representation of topographical features is an issue across all large- and medium-scale meteorological models, thus the generalization concept and process is of broad value. The generalization process results

Accepted for publication in *Bulletin of the American Meteorological Society.* DOI 10.1175/BAMS-D-21-0075.1.

in a GWC that is applicable over a larger geographic area, because it is no longer impacted by local-scale topography determined by the meteorological model.[2]

To add the impact of topography at fine resolution, the generalization process is then applied in reverse. A predicted wind climate (PWC) can be calculated by adding the better resolved topographic effects to the GWC, i.e., via perturbation of the mean wind speeds. In WAsP, the PWC is represented by a Weibull distribution and frequency of occurrence for each of the twelve directional sectors. The PWC is then used to derive different variables, such as the mean wind speed and the mean power density.

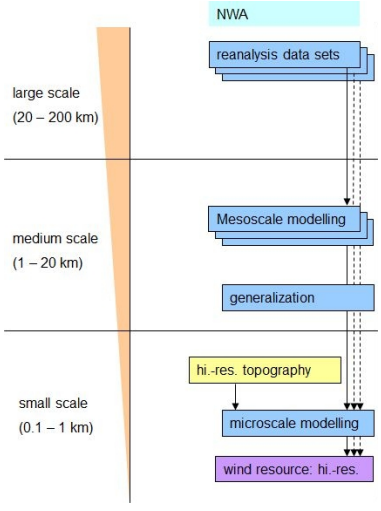

FIG. 2. Workflow schematic used in the Numerical Wind Atlas method.

3. Development of the Global Wind Atlas

Three major GWA versions, identified as such by changes to the underlying modeling system, have been released. GWA1, released in 2015, was funded as a three-year development and demonstration project by The Danish Energy Agency's EUDP[3]. GWA2, released in 2017, and GWA3, released in 2019, were developed with financing from ESMAP[4], a trust fund of the World Bank Group. Several minor versions, which include new features for users of the web application, were released for both GWA2 and GWA3. In this section, the methods of the mesoscale, generalization, and microscale

[2]The area of applicability is basically within a radius defined by the scale over which the ABL-mean pressure gradient itself does not change appreciably compared to the other two forces implicit in the geostrophic drag law, i.e., an effective Rossby-radius on the order of tens of kilometers. Complex terrain can reduce this area of applicability (see e.g. Kelly and Cavar 2023), an issue resolved by the resolution of the WRF simulations.

[3]Energy Technology Development and Demonstration Program : EUDP 11-II 64011-0347

[4]Energy Sector Management Assistance Program

Accepted for publication in *Bulletin of the American Meteorological Society.* DOI 10.1175/BAMS-D-21-0075.1.

modeling steps are described for each version of the GWA. Additionally, the web interface is briefly described, highlighting the functionality it provides.

a. Mesoscale modeling and generalization

The mesoscale modeling step changed the most with each GWA release, providing a more accurate representation of key physical processes. In GWA1, the mesoscale modeling step shown in Fig. 2 was not included. Instead, the generalization process was carried out directly on the MERRA[5] reanalysis dataset (Rienecker et al. 2011), which has a native resolution of $1/2^\circ \times 2/3^\circ$. The full MERRA period of 1979–2013 was used for estimating the wind climate, with a temporal resolution of 6 hours. Since the MERRA data is on a native lat-lon grid, several modifications to the NWA process were required. A detailed description of the selection of MERRA and the modeling process can be found in the project report (Badger et al. 2015).

In GWA2, mesoscale modeling was carried out using the Weather Research and Forecasting(WRF; Skamarock et al. 2008) mesoscale model, with a target resolution of 9 km. The WRF model output was created by Vortex FDC [6], using their standard operational setup. This includes the Rapid Radiative Transfer Model (RRTM) for the longwave (Mlawer et al. 1997) and shortwave radiation schemes (Iacono et al. 2008). The Eta similarity surface layer scheme (Janjić 1996), 5-layer thermal diffusion land surface scheme (Dudhia 1996), and Mellor-Yamada-Janjic planetary boundary layer scheme (Janjić 1994) were the only other schemes used. Parameterizations such as cumulus, snow cover effects, cloud effect to the optical depth in radiation, microphysics were disabled. The WRF's grid nudging was used on the outer domain to improve the initial conditions and guide the module during the integration period. Each WRF simulation was 24 hours long, with 6 hours spin-up, and outputs were saved every 30 minutes.

Approximately 420 WRF model domains were needed to cover the GWA area. Each WRF domain was run for a cluster of more than 720 days, which were selected to represent the full 10-year (2006–2015) long-term climatologies, as defined by the wind speed distribution and annual cycle. The input and boundary conditions were from the ERA-Interim reanalysis (Dee et al. 2011), with a resolution of $0.71^\circ \times 0.71^\circ$. To keep with the recommended resolution step-factor of three, WRF was run with two nested grids of 27 km and 9 km.

[5]Modern Era-Retrospective Analysis for Research and Applications
[6]https://vortexfdc.com/

Accepted for publication in *Bulletin of the American Meteorological Society.* DOI 10.1175/BAMS-D-21-0075.1.

In GWA3, the WRF model setup stayed the same, but several other advancements were included. Era-Interim was replaced by ERA5 (Hersbach et al. 2020), with higher resolution of $0.25° \times 0.25°$. Thus only a single WRF outer nest of 9 km was needed to reach the targeted 3 km resolution. With the increased resolution, 2,460 WRF model domains were required. Each domain was approximately $4° \times 4°$, with an area of $1°$ overlapping between neighboring simulations, leading to approximately 164 grid points in each direction. The outermost 10 grid points were discarded from each grid. The entire 10-year period from 2008–2017 was run.

Having the full time-series allowed additional wind statistics to be calculated, including annual, monthly, and hourly means and a "24×12 matrix". This matrix shows the hourly mean for each month of the year, allowing users to view how the diurnal pattern changes with the seasons for their location of interest.

The WRF model data on their native Lambert conformal conic grid projection were generalized for GWA3, using the approach described in Appendix A. To create a globally consistent grid of GWCs, the GWCs from each WRF model simulation were interpolated using natural neighbors interpolation to a regular lat-lon grid with a grid spacing of 0.0833°. In the area where 2 to 4 different WRF simulations overlap, we used a distance-weighted average based on the distance from the center of each simulation.

b. Microscale modeling

The microscale modeling was carried out using the WAsP Model (Troen and Petersen 1989) in all versions of the GWA with an output grid-spacing of 250 m. The WAsP Model uses the linear IBZ flow model (Troen 1990; Bowen and Mortensen 2004) for horizontal and vertical extrapolation of the wind based on high-resolution orographic and roughness length maps. The WAsP model was run using the WAsP Wind Resource Mapping Tool, Frogfoot, a distributed calculation platform, allowing for the simultaneous execution of many WAsP model simulations across different computers. Frogfoot was developed as part of the Finnish Wind Atlas (Tammelin et al. 2012) and Wind Atlas of South Africa projects (Mortensen et al. 2014a; Otto 2015).

For GWA1, version 11 of the WAsP model (Mortensen et al. 2014b) was used to calculate the wind resource at all land points between 85°N and 60°S and all water points within 30 km of coastlines based on the GSHHG[7] Wessel and Smith (1996). The 3-arc-second viewfinder Digital

[7]Global Self-consistent, Hierarchical, High-resolution Geography Database

Accepted for publication in *Bulletin of the American Meteorological Society.* DOI 10.1175/BAMS-D-21-0075.1.

TABLE 1. Land cover classes given by GlobCover and MODIS datasets and their corresponding assigned surface roughness lengths.

Description	GlobCover ID	MODIS ID	Roughness (m)
Water Bodies	210	0	0.0
Snow and ice	220	15	0.0004
Bare areas	200	16	0.005
Grassland & lichens/mosses	140	10	0.03
Sparse vegetation	150	None	0.05
Croplands	11, 14	12	0.1
Shrubland	130	6, 7	0.1
Wetlands	180	11	0.2
Natural vegetation	20, 30	14	0.3
Forest	160	None	0.5
Mosaic grassland / forest	120	9	0.5
Forest	170	None	0.6
Urban Areas	190	13	1.0
Forests	40, 50, 60, 70, 90, 100, 110	1, 2, 3, 4, 5, 8	1.5

Elevation Model (DEM)[8], which combines data from several sources to create a mostly void-filled dataset, was used. The roughness change dataset was derived from the GlobCover 2009 land cover dataset (Arino et al. 2008; Bontemps et al. 2011). The GlobCover dataset includes a land cover class of no-data, which was void filled using the coarser MODIS Land Cover Type product (MCD12Q1) (Friedl et al. 2010). The combined land cover dataset was converted to surface roughness lengths using a lookup table (Table 1) that was developed through a discussion with wind resource assessment experts. The experts looked at photographs and maps highlighting the areas represented by the different land cover classes to determine their mapping to roughness length. The 22 land cover classes were mapped to 14 roughness length values, with the seven forest classes being assigned a single value of surface roughness length. This conversion table is one of the major contributors to the uncertainty of the GWA, especially since the relationship between land cover and surface roughness in one part of the globe does not necessarily hold everywhere.

[8] http://viewfinderpanoramas.org/dem3.html

Accepted for publication in *Bulletin of the American Meteorological Society*. DOI 10.1175/BAMS-D-21-0075.1.

The microscale modeling setup was kept from GWA1 to GWA2, with the main focus of GWA2 being the mesoscale simulations, however GWA3 saw several updates. First, WAsP itself was upgraded to WAsP 12.3 (Mortensen et al. 2021). This allowed for the microscale modeling to make use of the updated air density model (Floors and Nielsen 2019), which used a dataset derived from the NCEP Climate Forecast System Reanalysis (CFSR) version 1 (Saha et al. 2010; Floors 2023), to get an accurate air density value anywhere in the world.

The largest changes in GWA3 were to the topographic data, with new sources for both the surface roughness and elevation data. The orographic data was replaced by void-filled SRTM[9] data between 60°N and 60°S, while viewfinder was still used north of 60°N. Despite being void-filled, several SRTM tiles had to be replaced with viewfinder data due to data artifacts. The artifacts were largely found in two areas: over the ocean extremely high elevations were found in areas of no land, suggesting that clouds were being mistaken for islands, and in mountainous regions, where the void-filling approach led to very steep gradients. Both of these issues could cause the WAsP flow model to fail. Additionally, a reexamination of the viewfinder data, revealed some gaps in the data. These were filled using cubic interpolation of the elevation in the south-north direction, as many of the void regions ran east-west. Both DEM datasets were provided as $1^\circ \times 1^\circ$ tiles, with 3 arc-second grid spacing.

The roughness length dataset was updated both in terms of the underlying land cover dataset and the look-up table. The GlobCover dataset used in the GWA1 and the GWA2 was replaced with the European Space Agency's Climate Change Initiative Land cover (CCI_LC) dataset v2.0.7 using the data for 2015 (ESA 2017). The ESA CCI_LC was selected as a relatively recent global land cover map, and used a similar classification system to GlobCover. Additionally, the land cover to roughness length table was updated, reducing the roughness length for many classes based on preliminary validations in South Africa, Vietnam, and Zambia.

Finally, to keep up with advancements in wind turbine technology, the amount of output data was increased. Additional heights (10 m and 200 m) were included to cover both small wind and the largest wind turbines. The calculation space was expanded to 200 km offshore, allowing the investigation of the wind resource for areas suitable for floating wind turbines.

[9] SRTMGL3v003 https://www.doi.org/10.5067/MEaSUREs/SRTM/SRTMGL3.003

Accepted for publication in *Bulletin of the American Meteorological Society.* DOI 10.1175/BAMS-D-21-0075.1.

TABLE 2. Land cover classes from the CCI_LC dataset and their corresponding assigned surface roughness lengths.

Description	CCI	Roughness (m)
Water	210	0.000
Snow and ice	220	0.003
Bare areas	200,201,202	0.005
Lichens/moss	140	0.010
Grass land	130	0.030
Sparse vegetation & small crops	20,150,151,152,153	0.050
Cropland & shrubland	10,11,110,120,180	0.100
Cropland & shrubland	12,30,100,121,122	0.200
Natural vegetation	40	0.300
Tree cover	170	0.600
Tree cover	62,160	0.800
Urban areas & Tree cover	60,61,190	1.000
Tree cover	80,81,82	1.200
Tree cover	50,70,71,72,90	1.500

c. Web application and derived quantities

Right from the start the GWA was designed to be distributed through a web platform allowing users to view the data in their browser. For GWA1, DTU developed the tool (Fig. 3), which was simpler in many ways to the current platform. Novel features included the ability for users to view wind statistics for custom defined areas by drawing a polygon on a map, and selecting a metric. Users could select many of the different model results to view on a map of the world, at different zoom levels, although restricted to a fixed color map with relatively coarse color resolution.

The web application saw a complete reinvention for the GWA2 (Fig. 4). The new site brought in experts in user interface design for map display and applications, with a goal to make the interface more user-friendly. As a result, the number of data layers was reduced through grouping and removing complex model output data, the ancillary graphs were moved to a sidebar to prevent covering the map, and data was provided for download. This layout for the site has remained in all subsequent versions.

Accepted for publication in *Bulletin of the American Meteorological Society*. DOI 10.1175/BAMS-D-21-0075.1.

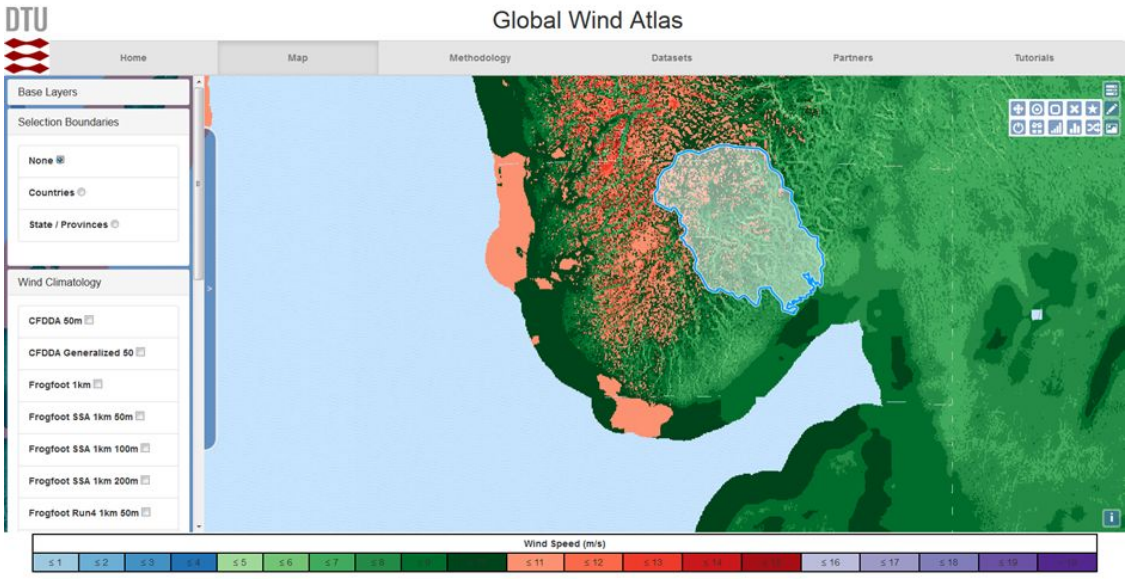

FIG. 3. Screenshot of the Web Application for GWA1. The mean wind speed at 100 m a.s.l. is shown and an administrative area of Norway is highlighted and used as part of spatial analysis of wind resources. The analysis tools are selected by the icons in the top-right of the window. The display of different layers is selected using the panel on the left of the window.

We also focused on adding derived data to the site to provide more value to GWA users. For the first time, turbine power information was added by including new layers of gross capacity factor (does not account for any losses e.g. wake), the calculation of which is described in Appendix B. These layers used the wind speed distribution data at 100 m above ground level (a.g.l) combined with power curves from three different turbines, Vestas V112-3.45MW, Vestas V126-3.45MW, and Vestas V136-3.45MW, which represent the three IEC turbine classes[10]. Enhanced wind roses, showing the sectors with the largest wind speed or power density, were also added.

Since the redesign, the web application has seen significant upgrades, allowing users to do more complex calculations, and interact more with the data. Some highlights include the ability to dynamically change color bars and the color-scale for each map layer (Fig. 5), and the ability to calculate a map of energy yield (see appendix B). In addition, the ability to download the data has been improved with each version. In GWA1, only the entire global dataset could be downloaded. Now users can download for individual countries, regions, or even custom areas that they select. Different reports have been added, including validation reports and offshore wind

[10] International Electrotechnical Commission (IEC) Standard 61400

Accepted for publication in *Bulletin of the American Meteorological Society.* DOI 10.1175/BAMS-D-21-0075.1.

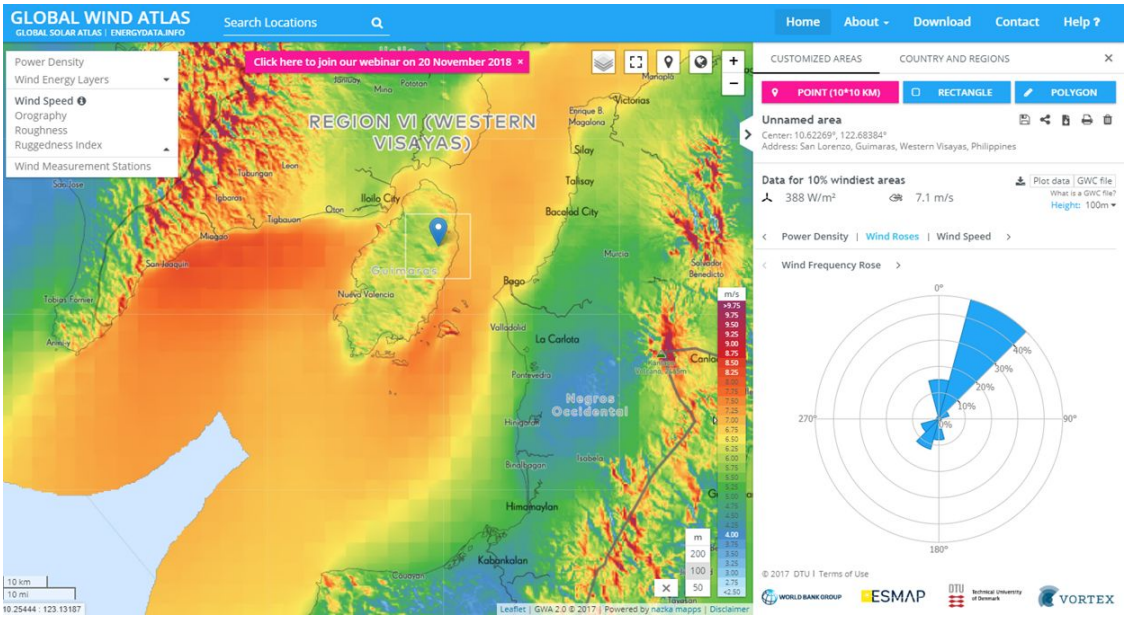

FIG. 4. Screenshot of the Web Application for GWA2. The mean wind speed at 100 m a.s.l is shown for a location on the island of Guimaras in the Philippines. Various key summary data are presented, for the location defined by the user, on the right-hand side of the window, including the wind rose, showing the frequency of occurrence of different direction sectors. Different layers can be selected using the panel on the left-hand side. Overall, there are more tools for navigating, selecting analysis, and downloading data and prepared graphics, compared to GWA1.

technical potential reports created by the World Bank. Locations and details of measurement campaigns, and access to the public wind measurement data used for the GWA validation are available via the web app, via links to the World Bank energydata.info webpages [11].

4. Validation

During the development of the GWA it has been important to indicate levels of confidence in the results. For example, we have included the Ruggedness Index (RIX) layer, which indicates to users where the orography is sufficiently complex to cause an expected increase in bias and uncertainty due to the effect of overestimated speed-up effects due to the linearized flow model (Bowen and Mortensen 1996, 2004; Dörenkämper et al. 2020). Additionally, the GWA datasets had validation efforts for each version, see e.g. Mortensen et al. (2017) and Mortensen (2021).

[11] https://energydata.info/dataset?q=wind+measurement+data

Accepted for publication in *Bulletin of the American Meteorological Society*. DOI 10.1175/BAMS-D-21-0075.1.

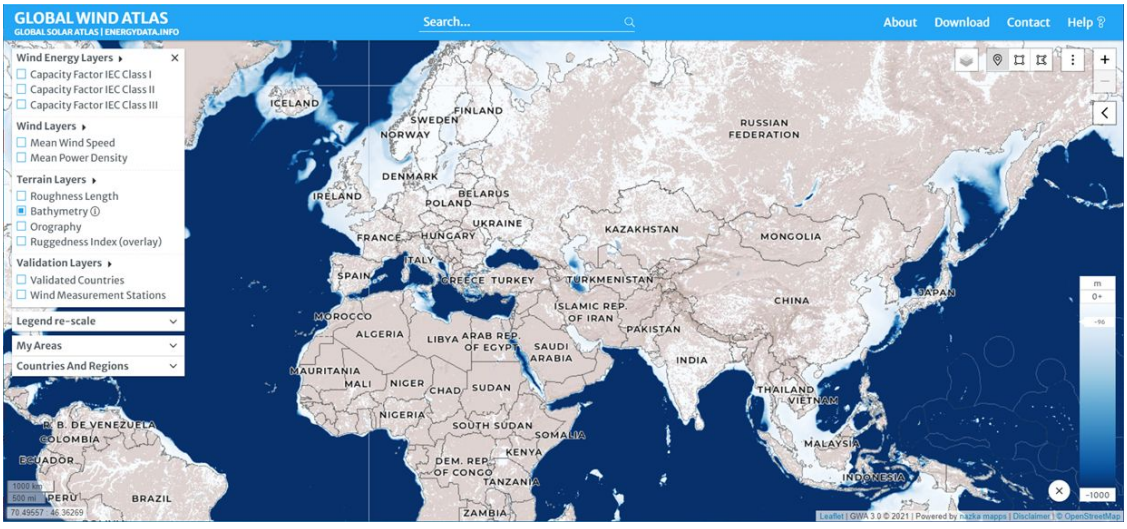

FIG. 5. Screenshot of the Web Application in the GWA3, where the sea depth layer (bathymetry) is shown. This layer was introduced in this version together with user-defined legend scale ranges, among many other features. The user-defined legend scaling allows users to create graphical representation of wind resources specifically for their need. For example, using specific wind power density data and bathymetry data ranges, allows for spatial consideration of different offshore wind resources, such as bottom-fixed and floating wind technologies.

As part of a drive to include validation as a more integrated part of the GWA and to increase its visibility, application, and value of ESMAP-funded measurement campaigns, GWA3 included an official validation approach. In the approach, the wind measurements are first truncated to full years, where possible, and then long-term adjusted to represent the 2008–2017 period using the wind index method (Thøgersen et al. 2007) with ERA5 data. This results in a long-term adjusted observed wind climate. The observed wind climate is then used to calculate a GWC using WAsP (v12.3) and high-quality topographic maps specific to the measurement site. The GWCs thus produced can be compared with the GWCs from the GWA for the same locations. This comparison provides a way to determine the confidence level of the GWA before the microscale modeling step. The GWC for each site can then be used to calculate a self-predicted PWC (predicted wind climate) using the same high-quality maps. This self-PWC is compared with the GWA-PWC to validate the final GWA results. Details of the procedure can be found on the Global Wind Atlas website [12]. Microscale fields from the GWA2 have also been used for bias correcting wind speed time series

[12] https://globalwindatlas.info/about/validation

Accepted for publication in *Bulletin of the American Meteorological Society.* DOI 10.1175/BAMS-D-21-0075.1.

for power system studies (Murcia et al. 2022; Gruber et al. 2022). These data compare well with European-wide large scale production data (Murcia et al. 2022).

The validation in GWA3 has been performed for 35 sites in six countries. For the PWC at 80 m there is a 14 % mean absolute bias and a −1 % mean bias on wind speed [13]. Countries with validated measurement sites are presented with a validation seal as part of their country summary. The seal includes the country-wide relative bias and standard deviation based on all validation sites in the country. Additionally, full reports of the validation can be downloaded, which provide details of the data and comparisons at the individual measurement sites. The report includes i) the long-term adjusted observed wind climate mean wind speeds, ii) the generalized wind climate data derived from measurements and derived from the GWA method, and iii) the predicted wind climate derived from the GWA method.

5. Usage of the GWA

The GWA gives ample possibilities for browsing and understanding the characteristics of wind climate around the world. Non-meteorologists and policymakers may use the maps to get an overview of the different wind resources from one country relative to another. Comparing wind resources for example for a country where the wind sector is already well-developed to one yet to develop. Thus the GWA provides a valuable starting point, and reference, before getting into greater details and commissioning further studies, including wind measurements.

Meteorologists, not in the wind sector, can use the GWA to investigate flow characteristics that capture all relevant meteorological scales, from global circulation, synoptic, mesoscale and microscale. This can also be valuable in educational settings. For example, from natural physical features in the landscape shaped by wind (e.g. desert dune formation and sand migration), to features of the built environment dictated by wind (e.g. airport runway orientations and sheltering features).

We give here an example of the use of the GWA for the Philippines to highlight the power of the data and web interface to explore, anywhere in the world, the behavior of wind characteristics. The example is a use case for an energy specialist wanting to investigate where wind resources are high and the reasons behind this.

[13]Note: Absolute bias is always positive, it is the magnitude of the bias

Accepted for publication in *Bulletin of the American Meteorological Society.* DOI 10.1175/BAMS-D-21-0075.1.

Figure 4 shows the mean wind speed for the island of Guimaras and surroundings. We also show the wind rose, which indicates a predominately NNE wind direction for the pinned location. With the GWA it is possible to explore further the reasons for this and explore the temporal characteristics of the wind resource. Figure 6a shows the terrain heights for a larger region than in Fig. 4. The terrain heights of the large islands exceed 1500 m above sea level. These terrain features are often associated with gap flows, which impact the wind climate of the region. Figure 6b shows that indeed, the mean wind speed map indicates the presence of gap flows, which increase the wind speeds between the large islands downwind of the gap. The gap flow is a feature captured by the mesoscale modeling part of the model chain.

In Figure 7a, which again zooms in on the island of Guimaras, it is possible to see the variation in mean wind speed on the island caused by the hill tops and ridges (due to orographic speed-up effects) and coastlines (low roughness in the predominantly upwind direction). These details are features captured by the microscale modeling of GWA.

Figure 7b highlights the temporal variation simulated in GWA3 through the 24×12 matrix showing the increased winds during the winter months. This knowledge is especially valuable for energy planners in determining the interplay and complementary between wind resources, other generation, and energy demand, with respective to season and daily variations.

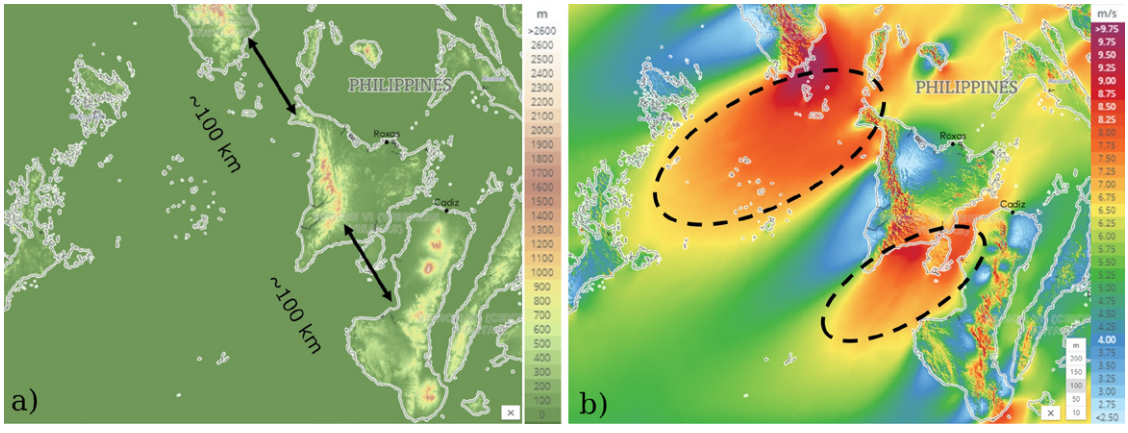

FIG. 6. (a) Screenshot from the GWA showing the orography for part of the Philippines. It shows parts of the large islands reaching up to 1500 m and higher. Also indicated on the figure is the approximate length scale between the large islands with high terrain. (b) Screenshot from the GWA showing the mean wind speed for the same area as (a). The higher wind speeds in and downwind of the gaps between the islands can be clearly seen.

Accepted for publication in *Bulletin of the American Meteorological Society.* DOI 10.1175/BAMS-D-21-0075.1.

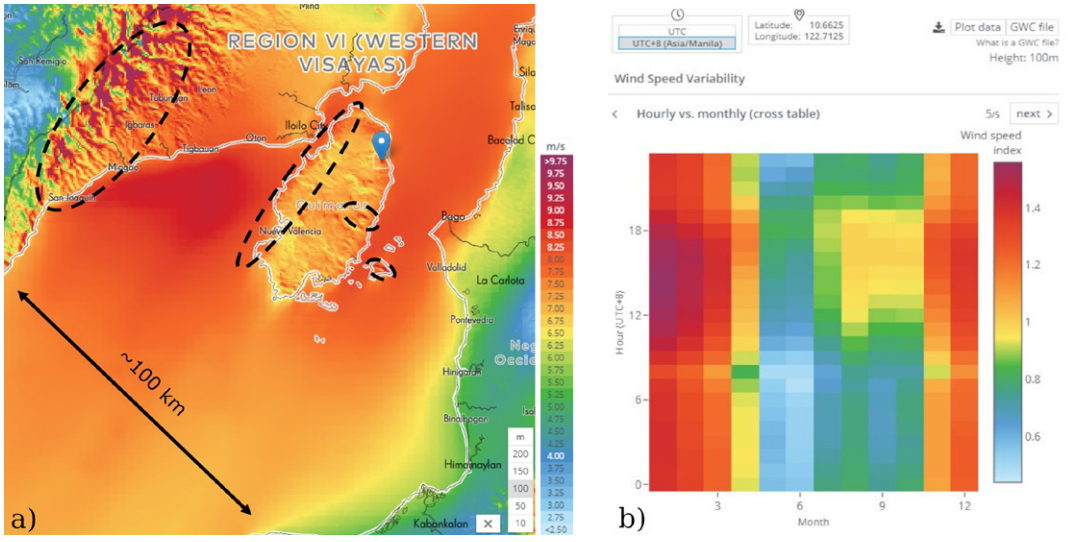

FIG. 7. (a) Screenshot from the GWA3 showing in more detail the variation of mean wind speed on Guimaras and around the gap flow in which the island is situated. Dashed ellipses indicate areas where the wind resources are enhanced by microscale effects, such as orography speed-up on hills and ridges and low roughness in the predominately upwind direction. (b) Screenshot from the GWA3 showing the variation of normalized mean wind speed for the marked location in (a) as a function of time of day (y-axis) and month of year (x-axis). It can be seen that the resource is most plentiful in the months November to March, and usually maximum in the local afternoon hours.

6. Conclusions and future directions

The first Global Wind Atlas was launched at a time when many countries were looking to increase their deployment of renewable energy and wanted to know to what extent there were wind resources in their country. By providing a high-resolution resource map using a homogeneous method everywhere in the world, the GWA has been able to provide a common starting website to answer that question, and avoided the need for each country to carry out their own wind atlas at an early stage of inquiry.

The development of the GWA will continue, with the aim to provide greater availability of relevant data and to increase accessibility (for example, in 2022 a multi-language version was launched). Future versions will include improved accuracy, increased dissemination of validation efforts, and increased relevance and value for user needs. As development in the wind energy sector evolves, the development of the GWA will most likely be:

Accepted for publication in *Bulletin of the American Meteorological Society*. DOI 10.1175/BAMS-D-21-0075.1.

Of general benefit and interest:

- To develop tools for the assessment of energy production for very large offshore wind farm clusters, including wake losses.
- To provide greater coverage over ocean basins in anticipation of the development of floating offshore wind deployment.
- To include more validation datasets, such as winds derived from remote sensing, and creation of a global uncertainty estimate.
- To provide information about other meteorological fields relevant for renewable energy to increase the application of the atlas in planning energy system modeling.
- To improve the accuracy of the mesoscale modeling, including improved handling of adjoining tile boundaries.
- To improve the accuracy of the microscale modeling through better topographic data, particularly roughness length modeling. Additionally, the inclusion of results from multiple mesoscale model levels is being explored to improve modeling of phenomena like low-level jets.
- To improve the microscale modeling, including exploring the use of more advanced Computational Fluid Dynamics (CFD) models to achieve better performance in areas of complex terrain.

Of specialist benefit and interest:

- To expand the web interface to include data layers for siting parameters, e.g. extreme winds, turbulence intensity, flow inclination, for use in determining wind turbine design requirements.
- To include other meteorological or environmental properties that may degrade wind turbine performance, e.g. icing and precipitation intensity.
- To include improved temporal information to give indicative time-series of wind generation to facilitate preliminary investigations of the integration of wind power in the power system and power market.

Accepted for publication in *Bulletin of the American Meteorological Society.* DOI 10.1175/BAMS-D-21-0075.1.

One of the challenges of the development of the GWA is the need to address a broad range of user needs, while at the same time remain a relatively easy and intuitive web application. The challenge of addressing energy generalists and wind energy specialists users can be met by i) providing the most generally relevant layers and summary data in a very upfront manner, and for download as graphics and reports, and ii) providing more technical layers and advanced tools in a slightly hidden manner, while also providing the raw data for download in GIS formats ready for subsequent user analysis. In this way, the mutual reinforcement of having a platform used both by generalists and experts will continue to be relevant and of value to the energy community at large.

Acknowledgments. The Global Wind Atlas version 1 was originally developed by a team consisting of Jake Badger [1], Neil Davis [1], Ray Drummond [6], Andrea Hahmann [1], Duncan Heathfield [6], Niels Gylling Mortensen [1] Marko Onninen [6] and Mark Kelly [1], with financial support from the Technology Development and Demonstration Program of the Danish Energy Agency (EUDP 11-II, 64011-0347).

Versions 2 and 3 of the Global Wind Atlas were developed by a team consisting of Jake Badger [1], Ides Bauwens [3], Pau Casso [2], Neil Davis [1], Andrea Hahmann [1], Søren Bo Krohn Hansen [5], Brian Ohrbeck Hansen [1], Duncan Heathfield [6], Oliver James Knight [4], Oriol Lacave [2], Gil Lizcano [2], Albert Bosch i Mas [2], Niels Gylling Mortensen [1], Bjarke Tobias Olsen [1], Marko Onninen [6], Albertine Potter Van Loon [4] and Patrick Volker [1], with financial support from the Energy Sector Management Assistance Program (ESMAP), a multi-donor trust fund administered by The World Bank.

1: DTU Wind Energy, 2: Vortex, 3: Nazka Mapps, 4: World Bank Group, 5: Søren Krohn Consulting, 6: World in a Box.

The Frogfoot system was developed by DTU for the Wind Atlas for South Africa (WASA) project, which is an initiative of the South African Department of Energy co-funded by the Royal Danish Embassy and UNDP-GEF. The WASA project is coordinated by South African National Energy Development Institute (SANEDI) and implemented by the following partners: Council for Scientific and Industrial Research (CSIR), University of Cape Town (UCT), South African Weather Service (SAWS) and DTU Wind Energy.

Data availability statement. Full terms and conditions for using Global Wind Atlas data are available on this webpage, https://globalwindatlas.info/about/TermsOfUse. Please read the Terms

Accepted for publication in *Bulletin of the American Meteorological Society.* DOI 10.1175/BAMS-D-21-0075.1.

of Use carefully before you start to use the GWA App or the Works. By using the GWA App, you accept and agree to be bound and abide by these Terms of Use. If you do not want to agree to these Terms of Use, you must not access the GWA App or use the Works. You are encouraged to use the GWA App and the Works to benefit yourself and others in creative ways. The Works are licensed under the Creative Commons Attribution 4.0 International license, CC BY 4.0, except where expressly stated that another license applies. To recognize the full partnership involved in developing the GWA App and Works, users are requested to use the following citation text: *"Global Wind Atlas 3, a free, web-based application developed, owned and operated by the Technical University of Denmark (DTU). The Global Wind Atlas is released in partnership with the World Bank Group, utilizing data provided by Vortex, using funding provided by the Energy Sector Management Assistance Program (ESMAP). For additional information: https://globalwindatlas.info"*

APPENDIX A

Generalization process

The generalization process starts by calculating the wind climate for each grid cell in the NWP model. The wind climate is defined as a tabular histogram with bins for both wind speed and direction (sector) and a wind rose consisting of the total occurrence of wind from each direction (sector); i.e., it is a discretized joint distribution of wind speed and direction.

Two pairs of direction-dependent generalization factors are calculated for each NWP model grid cell (Badger et al. 2014): the local impact of the NWP model orography on wind speed and direction (δA_o and $\delta \phi_o$, respectively), and the local impact of the NWP model roughness length on wind speed and direction (δA_r and $\delta \phi_r$) . It is very important that the NWP model orography and time-averaged roughness length are used (as opposed to local "microscale" elevations and roughnesses). By using the NWP topographic data, the generalization process removes the local impact of this coarser data on the wind. If high-resolution topographic data were used for this step, it would not correctly represent the topographic impact of the wind in the NWP model. The orographic factors are calculated using the linearized flow model LINCOM (Dunkerley et al. 2001). The roughness-change generalization factors are calculated using the WAsP roughness-change model based on Sempreviva et al. (1990), simulating the impact of internal boundary layers due to significant upstream roughness changes. The upstream roughness length, $\hat{z}_0$, is calculated

Accepted for publication in *Bulletin of the American Meteorological Society.* DOI 10.1175/BAMS-D-21-0075.1.

for each model grid cell and each wind direction (sector) using a weighted average of the roughness lengths for upstream grid cells using the approach from Troen and Petersen (1989). Badger et al. (2014) gives more information about the calculation of the generalization factors, and Hahmann et al. (2014) provides a comprehensive description of the generalization process itself.

These generalization factors are then applied to calculate the generalized wind speed through a multi-step process that removes the NWP-modeled impact of local orography and roughness length changes, and accounts for the representative roughness length of the NWP-derived wind climatology.

- Step 1: the impacts of orography and roughness length changes are removed, to calculate a corrected wind speed, $\hat{U}$. This wind speed is what would be expected for flat terrain and homogeneous upwind roughness length. Note however, that the geostrophic-scale upwind roughness length $\hat{z}_0$ is a function of direction (sector).

$$\hat{U} = \frac{U}{(1+\delta A_o)(1+\delta A_r)}. \tag{A1}$$

- Step 2: a friction velocity, $\hat{u}_*$, is calculated using the stability-corrected log profile (using the Monin-Obukhov wind profile and geostrophic drag law) (Troen and Petersen 1989; Kelly and Troen 2016), using the corrected wind speed $\hat{U}$ and upwind roughness length $\hat{z}_0$.

$$\hat{u}_* = \frac{\kappa \hat{U}}{\ln(z/\hat{z}_0)}, \tag{A2}$$

  where κ is the von Kármán constant and z is the height of the corrected wind speed.

- Step 3: using the friction velocity $\hat{u}_*$ and the the upwind roughness length $\hat{z}_0$, the geostrophic drag law (GDL) is applied to determine a representative geostrophic wind speed, $\hat{G}$.

$$\hat{G} = \frac{\hat{u}_*}{\kappa}\sqrt{\left(\ln\left[\frac{\hat{u}_*}{|f|\,\hat{z}_0}\right] - A\right)^2 + B^2}, \tag{A3}$$

  where $A = 1.8$ and $B = 4.5$ are two empirical factors, and f is the Coriolis parameter.

Accepted for publication in *Bulletin of the American Meteorological Society.* DOI 10.1175/BAMS-D-21-0075.1.

- Step 4: the GDL is applied again, this time using an iterative method, to determine a generalized friction velocity $\hat{u}_{*_g}$, using $\hat{G}$ (evaluated in A3) and a standardized roughness length, z_{0_g}.
- Step 5: the wind profile form is applied to determine the generalized wind speed, u_g, at a standardized height, z_g, for standardized roughness length, z_{0_g}. This wind speed is what would be expected for flat terrain and homogeneous roughness length everywhere, i.e. the upstream roughness length is no longer a function of direction (sector).

$$\hat{u_g} = \frac{\hat{u}_{*_g}}{\kappa} ln(z_g/\hat{z}_{0_g}), \tag{A4}$$

However, the parameters used to calculate $\hat{z}_0$ and roughness-change generalization factors were modified to ensure smooth generalized wind climate estimates across flat coastal zones. In the traditional NWA approach, the same number of mesoscale model grid points are used for calculating both of these parameters. However, it was found that for the finer grid spacing such as used in GWA3, more points were needed for the $\hat{z_0}$ calculation than for the roughness-change generalization factors.

The wind direction corrections are also applied with a direction change introduced via the vector form (velocity components) of the GDL.

The generalization process outlined above can be reversed to predict wind speed at a new location having different orography and roughness lengths. In that process the four direction-dependent generalization factors are calculated using the high-resolution digital elevation models (DEMs) and roughness length maps; the latter is also used for the upstream roughness length, $\hat{z}_0$. This is the process implemented in the WAsP model, described in Troen and Petersen (1989); Troen (1990); Landberg et al. (2003); Mortensen et al. (2006).

APPENDIX B

From wind to power

There are two main elements in the calculation of wind resources. The first is to determine the wind speed distribution for turbine site at hub height. The second is to convert that wind speed distribution into energy production, using the so-called turbine-specific power curve. Typically, it

Accepted for publication in *Bulletin of the American Meteorological Society.* DOI 10.1175/BAMS-D-21-0075.1.

is the long-term wind speed distribution that is convolved with the power curve to give the expected annual energy production. Figure B1 gives an example of a power curve. Air density has a role in the power curve, with lower density leading to lower energy production.

Power curves are turbine specific. In the GWA, three representative power curves have been applied from turbines that fall within each of the three IEC-classes of wind turbines (IEC 2020). The turbines from different classes are built with different robustness in their design to withstand normal operational and extreme conditions. Class I turbines are the most robust, while Class-III turbines will typically get the most energy production at lower wind speeds.

For specific assessment of wind farms, wind resource is usually stated as TWh per year. Another useful measure of wind resource is to state the capacity factor. This is the ratio of the annual energy production over the annual energy production if the wind turbines was operating at rated-power the whole year.

Accepted for publication in *Bulletin of the American Meteorological Society.* DOI 10.1175/BAMS-D-21-0075.1.

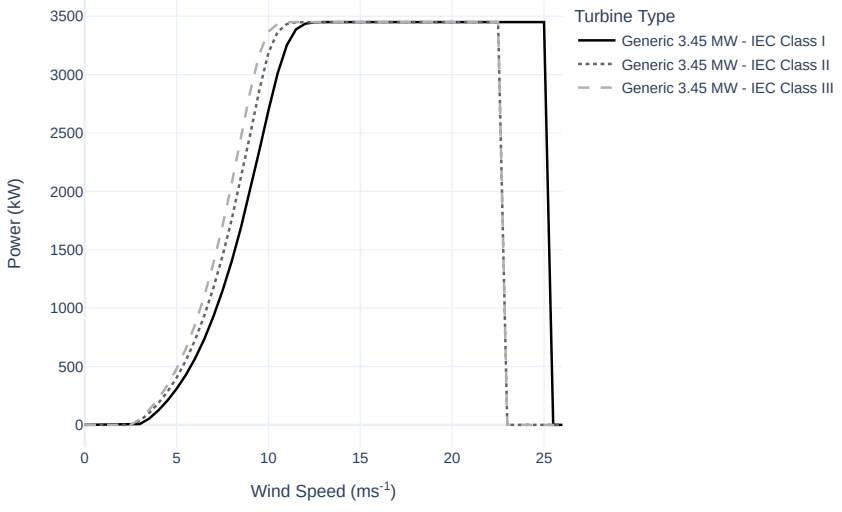

FIG. B1. The wind turbine power curves for turbines representing IEC Classes I (solid; black), II (short-dash; dark grey), and III (long-dash; light grey), used in the GWA. All turbines have the same rated power. Wind turbine power output (y-axis) is plotted as a function of the hub height wind speed (x-axis) for a fixed air density representative for a given site ($1.225\,\mathrm{kg\,m^{-3}}$ in this case). As wind speed increases, so too does the power generation, until rated-power is reached. In these specific examples, turbine models have a rated-power of 3.45 MW, reached at $13\,\mathrm{m\,s^{-1}}$, $12\,\mathrm{m\,s^{-1}}$ and $11\,\mathrm{m\,s^{-1}}$, for Class I, II and III respectively. Increasing wind speed beyond this does not increase generated power. The so-called cut-out speed, is the wind speed beyond which the turbine is shut down and power generation is zero.

Accepted for publication in *Bulletin of the American Meteorological Society.* DOI 10.1175/BAMS-D-21-0075.1.

APPENDIX C

Acronyms

CFSR	NCEP Climate Forecast System Reanalysis (CFSR) version 1
DEM	Digital Elevation Model
ESA CCI_LC	European Space Agency's Climate Change Initiative Land cover
ESMAP	Energy Sector Management Assistance Program
EUDP	Energy Technology Development and Demonstration Program
GDL	Geostrophic drag law
GIS	Geographic Information System
GSHHG	Global Self-consistent, Hierarchical, High-resolution Geography Database
GWA	Global Wind Atlas
GWC	Generalized wind climate
IEC	International Electrotechnical Commission
MERRA	Modern-Era Retrospective analysis for Research and Applications
MODIS	Moderate Resolution Imaging Spectroradiometer
NCEP	National Centers for Environmental Prediction
NWA	Numerical Wind Atlas
NWP	Numerical Weather Prediction
PWC	Predicted wind climate
RIX	Ruggedness Index
SRTM	Shuttle Radar Topography Mission
WRF	Weather Research and Forecasting
WAsP	Wind Atlas Analysis and Application Program

Accepted for publication in *Bulletin of the American Meteorological Society.* DOI 10.1175/BAMS-D-21-0075.1.

References

Arino, O., P. Bicheron, F. Achard, J. Latham, R. Witt, and J. L. Weber, 2008: Globcover: The most detailed portrait of earth. *European Space Agency Bulletin*, **2008**.

Badger, J., H. Frank, A. N. Hahmann, and G. Giebel, 2014: Wind-Climate Estimation Based on Mesoscale and Microscale Modeling: Statistical-Dynamical Downscaling for Wind Energy Applications. *J. Appl. Meteorol. Climatol.*, **53 (8)**, 1901–1919, https://doi.org/10.1175/JAMC-D-13-0147.1, URL http://journals.ametsoc.org/doi/abs/10.1175/JAMC-D-13-0147.1.

Badger, J., A. Hahmann, X. Larsén, M. Badger, M. Kelly, B. Olsen, and N. Mortensen, 2015: *The Global Wind Atlas: An EUDP project carried out by DTU Wind Energy*. DTU Wind Energy.

Bontemps, S., P. Defourny, E. V. Bogaert, V. Kalogirou, and J. R. Perez, 2011: Globcover 2009 products description and validation report. *ESA Bulletin*, **136**.

Bowen, A., and N. G. Mortensen, 1996: Exploring the limits of WAsP – the wind atlas analysis and application program. *1996 European Union wind energy conference. Proceedings*, A. Zervos, H. Ehmann, and P. Helm, Eds., H.S. Stephens and Associates, 584–587, 1996 European Wind Energy Conference and Exhibition, EWEC '96 ; Conference date: 20-05-1996 Through 24-05-1996.

Bowen, A., and N. G. Mortensen, 2004: *WAsP prediction errors due to site orography*. No. 995(EN), Denmark. Forskningscenter Risoe. Risoe-R.

Dee, D. P., and Coauthors, 2011: The ERA-Interim reanalysis: configuration and performance of the data assimilation system. *Quarterly Journal of the Royal Meteorological Society*, **137 (656)**, 553–597, https://doi.org/10.1002/qj.828, URL https://onlinelibrary.wiley.com/doi/10.1002/qj.828.

Dörenkämper, M., and Coauthors, 2020: The Making of the New European Wind Atlas – Part 2: Production and evaluation. *Geoscientific Model Development*, **13 (10)**, 5079–5102, https://doi.org/10.5194/gmd-13-5079-2020, URL https://gmd.copernicus.org/articles/13/5079/2020/.

Accepted for publication in *Bulletin of the American Meteorological Society.* DOI 10.1175/BAMS-D-21-0075.1.

Dudhia, J., 1996: A multi-layer soil temperature model for mm5. *Sixth Annual PSU/NCAR Mesoscale Model Users' Workshop*, Penn State University & National Center for Atmospheric Research.

Dunkerley, F., J. Moreno, T. Mikkelsen, and I. Griffiths, 2001: Lincom wind flow model: Application to complex terrain with thermal stratification. *Physics and Chemistry of the Earth Part B - Hydrology Oceans and Atmosphere*, **26 (10)**, 839–842, https://doi.org/10.1016/S1464-1909(01)00095-8.

ESA, 2017: Land Cover CCI Product User Guide Version 2. Tech. Rep. European Space Agency, URL https://maps.elie.ucl.ac.be/CCI/viewer/download/ESACCI-LC-Ph2-PUGv2_2.0.pdf.

Floors, R., and M. Nielsen, 2019: Estimating Air Density Using Observations and Re-Analysis Outputs for Wind Energy Purposes. *Energies*, **12 (11)**, 2038, https://doi.org/10.3390/en12112038, URL https://www.mdpi.com/1996-1073/12/11/2038.

Floors, R. R., 2023: CFSR data for air density calculations in WAsP. URL https://data.dtu.dk/articles/dataset/CFSR_data_for_air_density_calculations_in_WAsP/21967226, https://doi.org/10.11583/DTU.21967226.v1.

Frank, H., and L. Landberg, 1997: Modelling the wind climate of Ireland. *Boundary Layer Meteorology*, **85 (3)**, 359–378, https://doi.org/{10.1023/A:1000552601288}.

Friedl, M. A., D. Sulla-Menashe, B. Tan, A. Schneider, N. Ramankutty, A. Sibley, and X. Huang, 2010: MODIS Collection 5 global land cover: Algorithm refinements and characterization of new datasets. *Remote Sensing of Environment*, **114 (1)**, 168–182, https://doi.org/10.1016/j.rse.2009.08.016, URL https://linkinghub.elsevier.com/retrieve/pii/S0034425709002673.

Gruber, K., P. Regner, S. Wehrle, M. Zeyringer, and J. Schmidt, 2022: Towards global validation of wind power simulations: A multi-country assessment of wind power simulation from merra-2 and era-5 reanalyses bias-corrected with the global wind atlas. *Energy*, **238**, 121 520, https://doi.org/https://doi.org/10.1016/j.energy.2021.121520.

Hahmann, A., R. Floors, C. Lennard, D. Cavar, B. Olsen, N. Davis, N. Mortensen, and J. Hansen, 2021: *Mesoscale and Microscale Downscaling for the Wind Atlas of South Africa (WASA) Project: Phase 3*. No. E-0218, DTU Wind Energy E, DTU Wind Energy, Denmark.

Accepted for publication in *Bulletin of the American Meteorological Society.* DOI 10.1175/BAMS-D-21-0075.1.

Hahmann, A. N., J. Badger, C. L. Vincent, M. Kelly, P. J. H. Volker, and J. Refslund, 2014: Mesoscale modeling for the wind atlas for South Africa (WASA) Project. Tech. rep., DTU Wind Energy, 77 pp pp. URL http://orbit.dtu.dk/services/downloadRegister/107110172/DTU_Wind_Energy_E_0050.pdf.

Hersbach, H., and Coauthors, 2020: The ERA5 global reanalysis. *Quarterly Journal of the Royal Meteorological Society*, **146 (730)**, 1999–2049, https://doi.org/10.1002/qj.3803, URL https://onlinelibrary.wiley.com/doi/10.1002/qj.3803.

Iacono, M. J., J. S. Delamere, E. J. Mlawer, M. W. Shephard, S. A. Clough, and W. D. Collins, 2008: Radiative forcing by long-lived greenhouse gases: Calculations with the aer radiative transfer models. *Journal of Geophysical Research*, **113**, D13 103, https://doi.org/10.1029/2008JD009944.

IEA, 2021: Net zero by 2050. IEA, Paris, URL https://www.iea.org/reports/net-zero-by-2050.

IEC, 2020: *Standard 61400–1, Edition 4. Wind turbine generator systems – Part 1: Design requirements*. International Electrotechnical Comission, Geneva, Switzerland, 168pp pp.

Janjić, Z. I., 1994: The step-mountain eta coordinate model: Further developments of the convection, viscous sublayer, and turbulence closure schemes. *Monthly Weather Review*, **122**, 927–945, https://doi.org/10.1175/1520-0493(1994)122⟨0927:TSMECM⟩2.0.CO;2, URL http://journals.ametsoc.org/doi/abs/10.1175/1520-0493(1994)122⟨0927:TSMECM⟩2.0.CO;2?prevSearch=&searchHistoryKey=, mYJ Reference.

Janjić, Z. I., 1996: The surface layer in the ncep eta model. *Eleventh Conference on Numerical Weather Prediction*, Amer. Meteor. Soc., 354–355.

Kelly, M., and D. Cavar, 2023: Effective roughness and 'displaced' mean flow over complex terrain. *Bound.-Lay Meteorol.*, **186**, 93–123, https://doi.org/0.1007/s10546-022-00748-z.

Kelly, M., and I. Troen, 2016: Probabilistic stability and "tall" wind profiles: theory and method for use in wind resource assessment. *Wind Energy*, **19 (2)**, 227–241.

Landberg, L., N. G. Mortensen, O. Rathmann, and L. Myllerup, 2003: The similarity principle - on using models correctly. *European Wind Energy Conference and Exhibition Proceedings (CD-*

Accepted for publication in *Bulletin of the American Meteorological Society.* DOI 10.1175/BAMS-D-21-0075.1.

ROM. CD 2), European Wind Energy Association (EWEA), 3, 2003 European Wind Energy Conference and Exhibition, EWEC 2003 ; Conference date: 16-06-2003 Through 19-06-2003.

Lee, J. C. Y., and M. J. Fields, 2021: An overview of wind-energy-production prediction bias, losses, and uncertainties. *Wind Energy Science*, **6 (2)**, 311–365, https://doi.org/10.5194/wes-6-311-2021, URL https://wes.copernicus.org/articles/6/311/2021/.

Lundtang Petersen, E., I. Troen, S. Frandsen, and K. Hedegaard, 1981: *Danish Windatlas: A Rational Method of Wind Energy Siting*. No. 428, Denmark. Forskningscenter Risoe. Risoe-R, Risø National Laboratory.

Mlawer, E. J., S. J. Taubman, P. D. Brown, M. J. Iacono, and S. a. Clough, 1997: Radiative transfer for inhomogeneous atmospheres: Rrtm, a validated correlated-k model for the longwave. *Journal of Geophysical Research*, **102**, 16 663, https://doi.org/10.1029/97JD00237, URL http://doi.wiley.com/10.1029/97JD00237.

Mortensen, N. G., 2021: Global Wind Atlas 1, 2 & 3 – validations and uncertainties. WindEurope Electric City 2021 ; Conference date: 23-11-2021 Through 25-11-2021.

Mortensen, N. G., J. Badger, J. C. Hansen, E. Mabille, and Y. Spamer, 2014a: Large-scale, high-resolution wind resource mapping for wind farm planning and development in South Africa. *Proceedings of EWEA 2014*, European Wind Energy Association (EWEA), URL http://www.ewea.org/annual2014/, European Wind Energy Conference & Exhibition 2014, EWEA ; Conference date: 10-03-2014 Through 13-03-2014.

Mortensen, N. G., A. Bowen, and I. Antoniou, 2006: Improving WAsP predictions in (too) complex terrain. *Proceedings (online)*, European Wind Energy Association (EWEA), 2006 European Wind Energy Conference and Exhibition, EWEC 2006 ; Conference date: 27-02-2006 Through 02-03-2006.

Mortensen, N. G., N. Davis, J. Badger, and A. Hahmann, 2017: Global Wind Atlas – validation and uncertainty. URL https://windeurope.org/workshops/resource-assessment-2017/, WindEurope Resource Assessment Workshop 2017 ; Conference date: 16-03-2017 Through 17-03-2017.

Accepted for publication in *Bulletin of the American Meteorological Society.* DOI 10.1175/BAMS-D-21-0075.1.

Mortensen, N. G., D. Heathfield, O. Rathmann, and M. Nielsen, 2014b: *Wind Atlas Analysis and Application Program: WAsP 11 Help Facility*. Department of Wind Energy, Technical University of Denmark.

Mortensen, N. G., D. Heathfield, O. Rathmann, and M. Nielsen, 2021: *Wind Atlas Analysis and Application Program: WAsP 12 Help Facility*. DTU Wind Energy, Denmark.

Murcia, J. P., M. J. Koivisto, G. Luzia, B. T. Olsen, A. N. Hahmann, P. E. Sørensen, and M. Als, 2022: Validation of European-scale simulated wind speed and wind generation time series. *Applied Energy*, **305**, 117 794, https://doi.org/10.1016/j.apenergy.2021.117794.

Otto, A., 2015: *WIND ATLAS FOR SOUTH AFRICA: Phase 1*. South African National Energy Development Institute, Strathavon, Sandton, South Africa, 50 pp., URL https://wasaproject.info/docs/WASABooklet.pdf.

Rienecker, M. M., and Coauthors, 2011: MERRA: NASA's modern-era retrospective analysis for research and applications. *J. Clim.*, **24**, 3624–3648, https://doi.org/10.1175/JCLI-D-11-00015.1.

Saha, S., and Coauthors, 2010: The NCEP Climate Forecast System Reanalysis. *Bull. Am. Meteorol. Soc.*, **91 (8)**, 1015–1057, https://doi.org/10.1175/2010BAMS3001.1, URL http://journals.ametsoc.org/doi/abs/10.1175/2010BAMS3001.1.

Sempreviva, A., S. Larsen, N. G. Mortensen, and I. Troen, 1990: Response of neutral boundary-layers to changes of roughness. *Boundary-Layer Meteorology*, **50 (1-4)**, 205–225, https://doi.org/10.1007/BF00120525.

Skamarock, W. C., and Coauthors, 2008: A Description of the Advanced Research WRF Version 3. Tech. Rep. NCAR/TN–475+STR, National Center for Atmospheric Research.

Tammelin, B., and Coauthors, 2012: Production of the Finnish wind atlas. *Wind Energy*, 19–35, https://doi.org/10.1002/we.517, URL http://dx.doi.org/10.1002/we.517.

Thøgersen, M. L., M. Motta, T. Sørensen, and P. Nielsen, 2007: Measure-correlate-predict methods: case studies and software implementation. *European Wind Energy Conference & Exhibition*, 10.

Accepted for publication in *Bulletin of the American Meteorological Society.* DOI 10.1175/BAMS-D-21-0075.1.

Troen, I., 1990: A high resolution spectral model for flow in complex terrain. *9. Symposium on turbulence and diffusion*, N. Jensen, L. Kristensen, and S. Larsen, Eds., American Meteorological Society, United States, 417–420, 9th Symposium on Turbulence and Diffusion ; Conference date: 30-04-1990 Through 03-05-1990.

Troen, I., and E. L. Petersen, 1989: *European Wind Atlas*. Published for the Commission of the European Communities, Directorate-General for Science, Research, and Development, Brussels, Belgium by Risø National Laboratory.

van der Laan, M. P., M. Kelly, R. Floors, and A. Peña, 2020: Rossby number similarity of an atmospheric RANS model using limited-length-scale turbulence closures extended to unstable stratification. *Wind Energy Science*, **5 (1)**, 355–374, https://doi.org/10.5194/wes-5-355-2020.

Wessel, P., and W. H. F. Smith, 1996: A global, self-consistent, hierarchical, high-resolution shoreline database. *Journal of Geophysical Research: Solid Earth*, **101 (B4)**, 8741–8743, https://doi.org/10.1029/96JB00104, URL http://doi.wiley.com/10.1029/96JB00104.

Accepted for publication in *Bulletin of the American Meteorological Society.* DOI 10.1175/BAMS-D-21-0075.1.